Dynamic Modeling of Multi-phase Hybrid Stepper Motors.

Roberto Zanasi[1] and Marco Fei[2]

***Abstract*— The paper presents the dynamic modeling of Multi-phase Hybrid Stepper Motors (MHSM). The model is as general as possible and it is obtained using a Lagrangian approach in the frame of the Power-Oriented Graphs (POG) technique. The obtained dynamic models can be directly implemented in Simulink and they can be used to simulate also the Permanent Magnet and the Variable Reluctance stepper motors. Some simulation results are finally presented.**

I. INTRODUCTION

Stepper motors are used in a wide variety of industrial and automotive applications where precise positioning and repeatability of movement without position feedback are important [1]. Accurate motor models are mandatory to achieve high performance. The Finite Element Metod (FEM) is used to optimize the system geometry [2] while the lumped parameters models are used to design effective control strategies [3]-[5].

In this paper the model of a Multi-phase Hybrid Stepper Motors is presented. Using the Power-Oriented Graphs modeling technique the dynamic equations can be directly implemented in the Matlab/Simulink environment [7]-[10]. Moreover the general structure of the model allows to modify all the electrical and mechanical lumped parameters of the stepper motor (i.e. the number of phases, the shape of the rotor flux, etc..) without changing its structure.

The paper is organized as follows. Sec. II introduces the notations, Sec. III shows the details of the Multi-phase Hybrid Stepper Motors (MHSM) model in the fixed and rotating reference frame and finally in Sec. IV the control and the simulation results are presented.

II. NOTATIONS

The symbols $\overset{i}{\underset{1:n}{\|[\ R_i\ ]\|}}$ and $\|[\ R_i\ ]\|_{1:n}^{i}$ will denote the column and row vectors of the elements R_i. The full matrix of the elements $R_{i,j}$ will be denoted as follows:

$$\overset{i}{\underset{1:n}{\|[\ R_{i,j}\ ]\|}}_{1:m}^{j} = \begin{bmatrix} R_{11} & R_{12} & \cdots & R_{1m} \\ R_{21} & R_{22} & \cdots & R_{2m} \\ \vdots & \vdots & \ddots & \vdots \\ R_{n1} & R_{n2} & \cdots & R_{nm} \end{bmatrix}.$$

The symbol $\sum_{n=a:d}^{b} c_n = c_a + c_{a+d} + c_{a+2d} + \dots$ will be used to represent the sum of a succession of numbers c_n where the index n ranges from a to b with increment d.

[1]Roberto Zanasi[1] is with with the Department of Engineering "Enzo Ferrari", University of Modena and Reggio Emilia, Modena, Italy, e-mail: roberto.zanasi@unimore.it

[2]Marco Fei is with Borghi S.p.A., Castelfranco Emilia, Modena, Italy, e-mail: marco.fei86@gmail.com

III. MULTI-PHASE HYBRID STEPPER MOTORS

The basic scheme of a Multi-phase Hybrid Stepper Motor (MHSM) with delta-connected phases is shown in Fig. 1. The rotor is axially magnetized by the permanent-magnet enclosed between two cups (or section) with the same number of teeth. In this way the two sections have a uniform flux of opposite polarity; one is polarized north and the other one is polarized south. The teeth on the two cups are misaligned with each other by a half-tooth pitch so that a north pole tooth coincides with a south pole slot and vice versa. The stator has a whole number of main magnetic poles evenly distribute. Each pole is provided with a winding and it is cast-leaded with teeth having the same tooth pitch of the rotor. Therefore in this type of motor the torque is created by the electromagnetic and the reluctance effects. Indeed the interaction between the magnetic field of the permanent magnet and the magnetic field of the stator currents produces a magnetic flux in the air gap which aligns the rotor teeth to the stator.

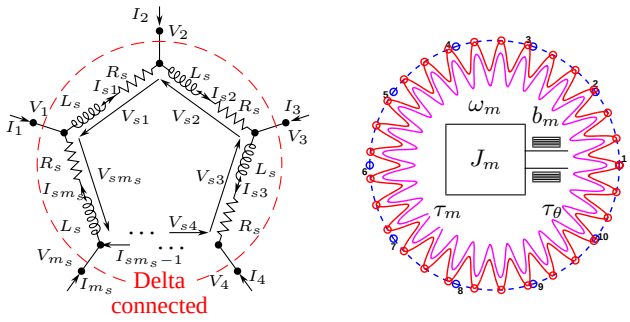

Fig. 1. Basic scheme of a MHSM with "delta-connected" stator phases.

The MHSM considered in this paper is supposed to be characterized by the parameters shown in Tab. I. The rotor has the magnetic structure shown in Fig. 2: 1) the first part of the rotor is rotated of angle $\theta_r = \frac{\pi}{m_r}$ with respect to the second part; 2) a permanent magnet is present between the two parts. An example is shown in Fig. 3.

The stator teeth are not uniformly distributed: the teeth of $(i+1)$-th stator phase, $i \in [1,\ 2,\ \dots,\ m_s]$, are rotated of the following electric angle:

$$\gamma_a = \frac{2\pi}{m_s\, q} = \frac{\gamma_s}{q} \tag{1}$$

with respect to the i-th stator phase, see Fig. 4.

TABLE I

PARAMETERS OF THE CONSIDERED MHSM.

m_s	number of stator phases: m_s is an odd number.
p	number of polar couples: $p \in \mathbb{N}$
q	number of rotor teeth of polar couple: $q = \alpha m_s$, $\alpha \in \mathbb{N}$.
m_r	number of rotor teeth: $m_r = p\,q$.
θ, θ_m	electric and rotor angular positions: $\theta = p\,\theta_m$.
ω, ω_m	electric and rotor angular velocities: $\omega = p\,\omega_m$.
I_i, I_{si},	line and stator phase currents for $i \in \{1, 2, \dots m_s\}$.
V_i, V_{si},	line and stator phase voltages for $i \in \{1, 2, \dots m_s\}$.
R_s	i-th stator phase resistance.
L_s	maximum value of the stator self induction coefficient.
M_{si}	maximum value of the i-th constant mutual inductance.
M_{ri}	maximum value of the i-th mutual inductance which is function of the electric angle θ.
J_m	rotor moment of inertia.
b_m	rotor linear friction coefficient.
τ_m	electromotive torque acting on the rotor.
τ_d	maximum detent torque due to the magnet when $I_{si} = 0$.
τ_e	external load torque acting on the rotor.
γ_s	stator basic angular displacement: $\gamma_s = 2\pi/m_s$.

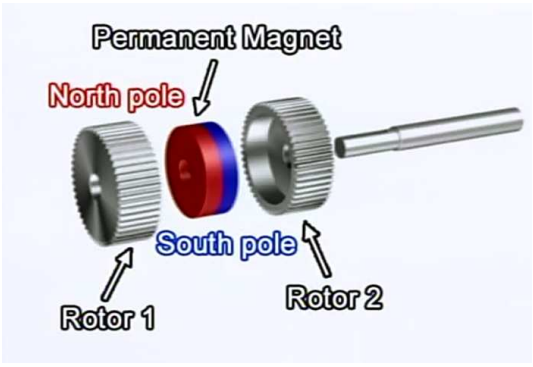

Fig. 2. Magnetic structure of the rotor.

A. Dynamic model of a MHSM.

Let ${}^t\mathbf{I}_l$, ${}^t\mathbf{V}_,$, ${}^t\mathbf{I}_s$ and ${}^t\mathbf{V}_s$ denote the "*line*" and "*stator*" current and voltage vectors in the static reference frame Σ_t:

$${}^t\mathbf{I}_l = \begin{bmatrix} I_1 \\ I_2 \\ \vdots \\ I_{m_s} \end{bmatrix}, \quad {}^t\mathbf{V}_l = \begin{bmatrix} V_1 \\ V_2 \\ \vdots \\ V_{m_s} \end{bmatrix}, \quad {}^t\mathbf{I}_s = \begin{bmatrix} I_{s1} \\ I_{s2} \\ \vdots \\ I_{sm_s} \end{bmatrix}, \quad {}^t\mathbf{V}_s = \begin{bmatrix} V_{s1} \\ V_{s2} \\ \vdots \\ V_{sm_s} \end{bmatrix}.$$

If the stator phases are delta-connected:

$${}^t\mathbf{V}_s = {}^t\mathbf{T}_\Delta\, {}^t\mathbf{V}_l, \qquad {}^t\mathbf{I}_l = {}^t\mathbf{T}_\Delta^{\mathrm{T}}\, {}^t\mathbf{I}_s \tag{2}$$

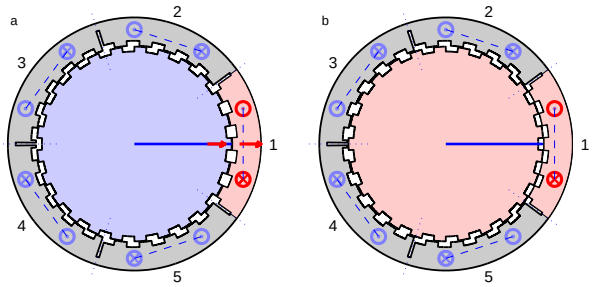

Fig. 3. The two parts of the rotor: $m_s = 5$, $m_r = q = 25$ and $p = 1$.

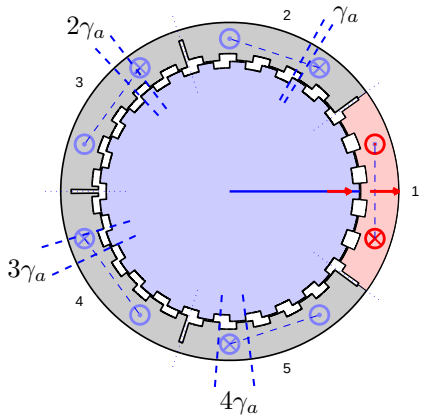

Fig. 4. MHSM with $m_s = 5$, $m_r = q = 25$ and $p = 1$. The teeth of the i-th stator phase are rotated of angle $i\gamma_a$ with respect to the 1-st stator phase.

where matrix ${}^t\mathbf{T}_\Delta$ is defined as follows:

$${}^t\mathbf{T}_\Delta = \Big\| \big[{}^tT^\Delta_{i,j} \big] \Big\|_{1:m_s}^{i} \; {}_{1:m_s}^{j}, \qquad {}^tT^\Delta_{i,j} = \begin{cases} 1 & \text{if } i = j \\ -1 & \text{if } i = j - 1 \\ -1 & \text{if } (i,j) = (m_s, 1) \\ 0 & \text{otherwise} \end{cases} \tag{3}$$

For $m_s = 5$ matrix ${}^t\mathbf{T}_\Delta$ has the following structure:

$${}^t\mathbf{T}_\Delta = \begin{bmatrix} 1 & -1 & 0 & 0 & 0 \\ 0 & 1 & -1 & 0 & 0 \\ 0 & 0 & 1 & -1 & 0 \\ 0 & 0 & 0 & 1 & -1 \\ -1 & 0 & 0 & 0 & 1 \end{bmatrix}.$$

From (2) and (3) it follows that: $\sum_{i=1}^{m_s} V_{si} = 0$, and $\sum_{i=1}^{m_s} I_i = 0$. Under the assumptions of regularity of the design and no iron saturation, the electro-mechanical state space equations of the considered MHSM obtained using a Lagrangian approach, see [6], are the following:

$$\begin{aligned} &\underbrace{\left[\begin{array}{c|c} {}^t\mathbf{L}_s(\theta) & \mathbf{0} \\ \hline \mathbf{0} & J_m \end{array}\right]}_{{}^t\mathbf{L}({}^t\mathbf{q})} \underbrace{\left[\begin{array}{c} {}^t\dot{\mathbf{I}}_s \\ \hline \dot{\omega}_m \end{array}\right]}_{{}^t\ddot{\mathbf{q}}} = \dots \\ &\underbrace{-\left[\begin{array}{c|c} {}^t\mathbf{R}_s + {}^t\mathbf{N}_s(\theta, \omega_m) & {}^t\mathbf{K}_\tau(\theta, {}^t\mathbf{I}_s) \\ \hline -{}^t\mathbf{K}_\tau^{\mathrm{T}}(\theta, {}^t\mathbf{I}_s) & b_m \end{array}\right]}_{{}^t\mathbf{A}(\theta, \omega_m, {}^t\mathbf{I}_s)} \underbrace{\left[\begin{array}{c} {}^t\mathbf{I}_s \\ \hline \omega_m \end{array}\right]}_{{}^t\dot{\mathbf{q}}} + \underbrace{\left[\begin{array}{c} {}^t\mathbf{V}_s \\ \hline -\tau_\theta \end{array}\right]}_{{}^t\mathbf{V}} \end{aligned} \tag{4}$$

where ${}^t\mathbf{R}_s = p\,R_s\,\mathbf{I}_{m_s}$ is the resistance diagonal matrix and

$$\begin{aligned} {}^t\mathbf{K}_\tau(\theta, {}^t\mathbf{I}_s) &= {}^t\mathbf{H}_s(\theta)\, {}^t\mathbf{I}_s + {}^t\mathbf{K}_c(\theta) \\ {}^t\mathbf{N}_s(\theta, \omega_m) &= {}^t\mathbf{H}_s(\theta)\, \omega_m \\ \tau_\theta &= \tau_d \sin(2q\theta) + \tau_e \end{aligned} \tag{5}$$

Matrices ${}^t\mathbf{H}_s(\theta)$ and ${}^t\mathbf{K}_c(\theta)$ are defined as follows:

$${}^t\mathbf{H}_s(\theta) = \frac{1}{2}\, p\, \frac{\partial\, {}^t\mathbf{L}_s(\theta)}{\partial\, \theta}, \qquad {}^t\mathbf{K}_c(\theta) = p \frac{\partial\, {}^t\mathbf{\Phi}_c(\theta)}{\partial \theta} \tag{6}$$

where ${}^t\mathbf{L}_s(\theta)$ is the motor inductance matrix and ${}^t\mathbf{\Phi}_c(\theta)$ is the magnetic flux vector concatenated with the stator phases. Since the air-gap is nonuniform, the inductance

matrix ${}^t\mathbf{L}_s(\theta)$ varies with rotor angular position and it has the following structure:

$$ {}^t\mathbf{L}_s(\theta) = {}^t\mathbf{L}_{sc} + {}^t\mathbf{L}_{s\theta} \tag{7} $$

where ${}^t\mathbf{L}_{sc}$ is the stator inductance matrix:

$$ {}^t\mathbf{L}_{sc} = p \left\| \left[L_{s0}\delta(i-j) + \sum_{n=1:2}^{m_s-2} M_{sn}\cos(n(i-j)\gamma_s) \right] \right\|_{0:m_s-1}^{i,j} \tag{8} $$

and ${}^t\mathbf{L}_{s\theta}$ is the rotor inductance matrix, see App. V:

$$ {}^t\mathbf{L}_{s\theta} = p \left\| \left[\sum_{n=1:2}^{m_s-2} M_{rn}\cos(2nq\theta - n(q-1)(i+j)\gamma_s) \right] \right\|_{0:m_s-1}^{i,j} \tag{9} $$

The term L_{s0} in (8) is defined as follows:

$$ L_{s0} = L_s - \sum_{n=1:2}^{m_s-2} M_{sn}. $$

The structure of flux vector ${}^t\mathbf{\Phi}_c(\theta)$ is, see App. VI:

$$ {}^t\mathbf{\Phi}_c(\theta) = \left\| \left[\sum_{n=1:2}^{\infty} \Psi_n \cos(nq\theta - nh(q-1)\gamma_s) \right] \right\|_{0:m_s-1}^{h}. \tag{10} $$

From (6), (7) and (10) it follows that:

$$ {}^t\mathbf{H}_s(\theta) = -p^2 \sum_{n=1:2}^{m_s-2} M_{rn} nq \left\| \left[\sin(2nq\theta - n(q-1)(i+j)\gamma_s) \right] \right\|_{0:m_s-1}^{i,j} $$

and

$$ {}^t\mathbf{K}_c(\theta) = -p \sum_{n=1:2}^{m_s-2} nq\Psi_n \left\| \left[\sin(nq\theta - n(q-1)h\gamma_s)) \right] \right\|_{0:m_s-1}^{h}. $$

Let ${}^t\mathbf{T}_\omega$ denote the following transformation matrix:

$$ {}^t\mathbf{T}_\omega = \sqrt{\frac{2}{m_s}} \left[\left\| \left[\cos(\alpha_k^h(\theta)) \quad \sin(\alpha_k^h(\theta)) \right] \right\|_{0:m_s-1}^{h,\,1:2:m_s-2,\,k} \quad \left\| \left[\tfrac{1}{\sqrt{2}} \right] \right\|_{0:m_s-1}^{h} \right] \tag{11} $$

where $\alpha_k^h(\theta) = k(qh\gamma_s - (q-1)\theta)$. Applying the state space transformation ${}^t\mathbf{I}_s = {}^t\mathbf{T}_\omega\, {}^\omega\mathbf{I}_s$ to system (4) one obtains the following transformed system:

$$ \underbrace{\left[\begin{array}{c|c} {}^\omega\mathbf{L}_s & 0 \\ \hline 0 & J_m \end{array} \right]}_{{}^\omega\mathbf{L}} \underbrace{\left[\begin{array}{c} {}^\omega\dot{\mathbf{I}}_s \\ \hline \dot{\omega}_m \end{array} \right]}_{{}^\omega\dot{\mathbf{q}}} = \dots $$

$$ \underbrace{-\left[\begin{array}{c|c} {}^\omega\mathbf{R}_s + {}^\omega\mathbf{N}_s(\omega_m) + {}^\omega\mathbf{L}_s\, {}^\omega\mathbf{J}_s(\omega_m) & {}^\omega\mathbf{K}_\tau({}^\omega\mathbf{I}_s) \\ \hline -{}^\omega\mathbf{K}_\tau^{\mathrm{T}}({}^\omega\mathbf{I}_s) & b_m \end{array} \right] \left[\begin{array}{c} {}^\omega\mathbf{I}_s \\ \hline \omega_m \end{array} \right]}_{{}^\omega\mathbf{A}(\omega_m, {}^\omega\mathbf{I}_s)} + \underbrace{\left[\begin{array}{c} {}^\omega\mathbf{V}_s \\ \hline -\tau_\theta \end{array} \right]}_{{}^\omega\mathbf{V}} \tag{12} $$

where ${}^\omega\mathbf{I}_s = {}^t\mathbf{T}_\omega^{\mathrm{T}}\, {}^t\mathbf{I}_s$, ${}^\omega\mathbf{L}_s = {}^t\mathbf{T}_\omega^{\mathrm{T}}\, {}^t\mathbf{L}_s\, {}^t\mathbf{T}_\omega$, ${}^\omega\mathbf{N}_s(\omega_m) = {}^t\mathbf{T}_\omega^{\mathrm{T}}\, {}^t\mathbf{N}_s\, {}^t\mathbf{T}_\omega$, ${}^\omega\mathbf{R}_s = {}^t\mathbf{T}_\omega^{\mathrm{T}}\, {}^t\mathbf{R}_s\, {}^t\mathbf{T}_\omega$, ${}^\omega\mathbf{J}_s(\omega_m) = {}^t\mathbf{T}_\omega^{\mathrm{T}}\, {}^t\dot{\mathbf{T}}_\omega$, ${}^\omega\mathbf{K}_\tau({}^\omega\mathbf{I}_s) = {}^t\mathbf{T}_\omega^{\mathrm{T}}\, {}^t\mathbf{K}_\tau$ and ${}^\omega\mathbf{V}_s = {}^t\mathbf{T}_\omega^{\mathrm{T}}\, {}^t\mathbf{V}_s$. The Power-Oriented Graphs (POG) block scheme of the transformed system (12) is shown in Fig. 5. Details on the POG modeling technique can be found in [7]. The transformed matrix ${}^\omega\mathbf{L}_s$ is constant and diagonal:

$$ {}^\omega\mathbf{L}_s = {}^\omega\mathbf{T}_t\, {}^t\mathbf{L}_s\, {}^t\mathbf{T}_\omega = \left[\begin{array}{cc} \left\| \left[\begin{array}{cc} p\,L_{dk} & 0 \\ 0 & p\,L_{qk} \end{array} \right] \right\|_{1:2:m_s-2}^{k} & \mathbf{0} \\ \mathbf{0} & pL_{s0} \end{array} \right] \tag{13} $$

where

$$ L_{dk} = L_{sk} + \frac{m_s}{2} M_{rk}, \qquad L_{qk} = L_{sk} - \frac{m_s}{2} M_{rk}. \tag{14} $$

$$ L_{sk} = L_{s0} + \frac{m_s}{2} M_{s,r(k)} \tag{15} $$

Function $r(k)$ in (15) transforms the index k into index $r(k)$ according to the following "k2r" Matlab routine:

```
%%%%%%%%%%%%%%%%%%%%%%%%%%%%%%%%%%%%%%%%%%%%%%%%%%%%%%%%
function r=k2r(k,q,ms)
for r=1:2:q-2
    if (delta(k*(q-1)+r,0,ms)+...
        delta(k*(q-1)-r,0,ms))==1
        return
    end
end;  return
%%%%%%%%%%%%%%%%%%%%%%%%%%%%%%%%%%%%%%%%%%%%%%%%%%%%%%%%
function delta=delta(n,k,q)
delta=0; if mod(n-k,q)==0; delta=1; end
return
%%%%%%%%%%%%%%%%%%%%%%%%%%%%%%%%%%%%%%%%%%%%%%%%%%%%%%%%
```

The result given in (13) can obtained only if: a) m_s is an odd number; b) $q-1$ is not a multiple of any factor p of m_s: $q-1 \neq \alpha p$ where $\alpha \in \mathbb{N}$ and p is any factor of parameter m_s. It can be proved that the transformed matrix ${}^\omega\mathbf{H}_s = {}^t\mathbf{T}_\omega^{\mathrm{T}}\, {}^t\mathbf{H}_s\, {}^t\mathbf{T}_\omega$ is symmetric and constant:

$$ {}^\omega\mathbf{H}_s = \left[\begin{array}{cc} \left\| \left[\begin{array}{cc} 0 & p^2kq\frac{m_s}{2}M_{rk} \\ p^2kq\frac{m_s}{2}M_{rk} & 0 \end{array} \right] \right\|_{1:2:m_s-2}^{k} & \mathbf{0} \\ \mathbf{0} & 0 \end{array} \right]. \tag{16} $$

and the transformed vector ${}^\omega\mathbf{K}_c = {}^t\mathbf{T}_\omega^{\mathrm{T}}\, {}^t\mathbf{K}_c$ is constant:

$$ {}^\omega\mathbf{K}_c = \left[\begin{array}{c} \left\| \left[\begin{array}{c} 0 \\ pq\sqrt{\frac{m_s}{2}}k\Psi_k \end{array} \right] \right\|_{1:2:m_s-2}^{k} \\ 0 \end{array} \right]. \tag{17} $$

From (5) and (16) it follows that matrix ${}^\omega\mathbf{M}_s(\omega_m) = {}^\omega\mathbf{N}_s(\omega_m) + {}^\omega\mathbf{L}_s\, {}^\omega\mathbf{J}_s(\omega_m)$ in (12) has the following skew-symmetric form:

$$ {}^\omega\mathbf{M}_s(\omega_m) = \left[\begin{array}{cc} \left\| \left[\begin{array}{cc} 0 & -p^2kqL_{sk} \\ p^2kqL_{sk} & 0 \end{array} \right] \right\|_{1:2:m_s-2}^{k} & \mathbf{0} \\ \mathbf{0} & 0 \end{array} \right] \omega_m \tag{18} $$

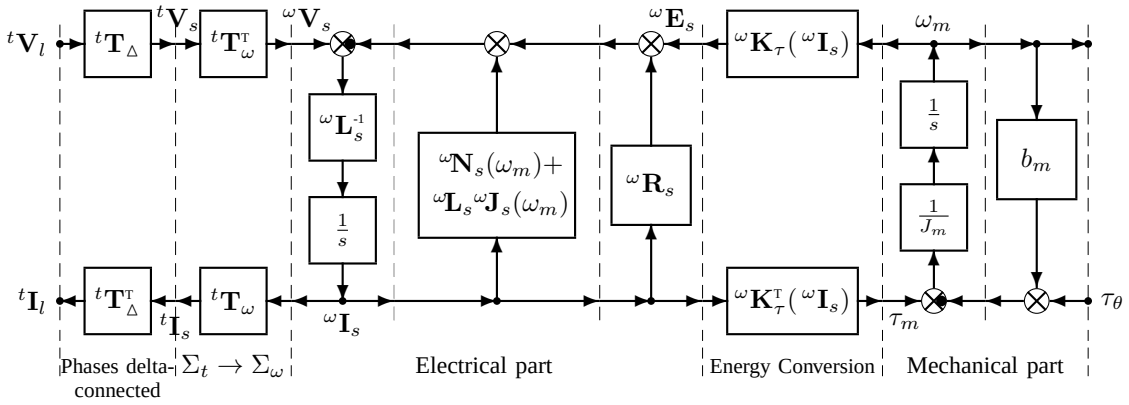

Fig. 5. POG block scheme of the hybrid multi-phase stepper motor in the transformed reference frame Σ_ω.

From (5) and (17) it follows that vector ${}^{\omega}\mathbf{K}_\tau = {}^{\omega}\mathbf{K}_\tau({}^{\omega}\mathbf{I}_s)$ has the following structure:

$$ {}^{\omega}\mathbf{K}_\tau = \begin{bmatrix} \left\| \begin{bmatrix} p^2 kq \frac{m_s}{2} M_{rk} I_{qk} \\ p^2 kq \frac{m_s}{2} M_{rk} I_{dk} + pq\sqrt{\frac{m_s}{2}} k \Psi_k \end{bmatrix} \right\|_{1:2:m_s-2}^{k} \\ 0 \end{bmatrix} = \begin{bmatrix} \left\| \begin{bmatrix} K_{dk} \\ K_{qk} \end{bmatrix} \right\|_{1:2:m_s-2}^{k} \\ 0 \end{bmatrix} \tag{19} $$

The proofs and the mathematical details of results (13), (16), (17), (18) and (19) can be found on the web at the address: http://www.dii.unimo.it/∼zanasi/ELECOM/Details.pdf.

The final transformed system has the structure shown in (20) in Fig. 6. The parameters L_{dk}, L_{qk}, L_{sk}, K_{dk} and K_{qk} are defined in (14), (15) and (19). When $m_s = 5$, the equations (20) have the structure shown in (21) in Fig. 6. From (21) it is evident that when ω_m is constant the first five equations of system (21) are linear and decoupled. From (19) it follows that the motor electromagnetic torque τ_m is:

$$ \begin{aligned} \tau_m &= {}^{\omega}\mathbf{K}_\tau^{\mathrm{T}}\, {}^{\omega}\mathbf{I}_s = {}^{\omega}\mathbf{I}_s^{\mathrm{T}}\, {}^{\omega}\mathbf{H}_s^{\mathrm{T}}\, {}^{\omega}\mathbf{I}_s + {}^{\omega}\mathbf{K}_c^{\mathrm{T}}\, {}^{\omega}\mathbf{I}_s \\ &= \sum_{k=1:2}^{m_s-2} pqk\sqrt{m_s}\left(p\sqrt{m_s} M_{rk} I_{dk} + \frac{\Psi_k}{\sqrt{2}} \right) I_{qk} \end{aligned} \tag{22} $$

When $\Psi_k = 0$, the motor torque τ_m is a quadratic function of the current vector ${}^{\omega}\mathbf{I}_s$. From (22) it is evident that the motor torque τ_m can be generated in $(m_s - 1)/2$ different ways which are obtained for $k \in \{1, 3, 5, \ldots, m_s{-}2\}$. Each bi-dimensional subsystem can generate torque independently from the others.

IV. Simulations

The dynamic model described in the previous section has been implemented in Simulink together with a current and a velocity cascade control, see Fig. 7. The parameters used in simulations are shown in Tab. II. The values of these parameters are not the "typical ones" for a commercial MHS motor and are used in this section only to test the correct behavior of the proposed dynamic model. The physical structure of the considered MHSM is shown in Fig. 8. In simulation the following current control law has been used:

$$ {}^{\omega}\mathbf{V}_s = {}^{\omega}\mathbf{V}_F - \mathbf{K}_d({}^{\omega}\mathbf{I}_s - {}^{\omega}\mathbf{I}_d) \tag{23} $$

TABLE II

Parameters of the considered MHSM.

m_s	5	p	2
q	25	m_r	50
R_s	1 Ω	L_s	5 mH
M_{s1}, M_{s3}	[4, 1.6] mH	M_{r1}, M_{r3}	[1.2, 0.4] mH
J_m	1.6 kg m^2	b_m	0.5 Nm s/rad
τ_d	0 Nm	τ_e	10 Nm
K_{d1}, K_{q1}, K_{c1},	[0.84, 0.48, 0.423]	$-\sigma_c \pm j\omega_c$	$-30 \pm j20$
K_{d2}, K_{q2}, K_{c2}	[0.36, 0.24, 0.196]	K_0,	0
Ψ_1, Ψ_3	[1.2, 0.4] Wb	α_1, α_3	[0.7, 0.3]
ω_{dm}	100 rpm	K_ω	150
τ_{max}	40 Nm	$\bar{I}_{m_s}$	0

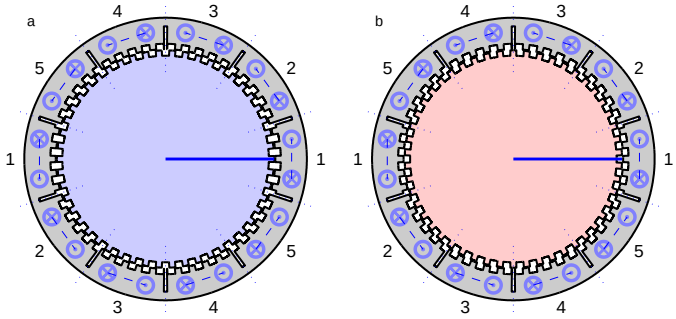

Fig. 8. Structure of a MHSM with $m_s = 5$, $q = 25$, $p = 2$ and $m_r = 50$.

where ${}^{\omega}\mathbf{I}_d$ is the desired current vector and ${}^{\omega}\mathbf{V}_F$ is the feed-forward action:

$$ {}^{\omega}\mathbf{V}_F = [{}^{\omega}\mathbf{R}_s + {}^{\omega}\mathbf{N}_s(\omega_m) + {}^{\omega}\mathbf{L}_s\, {}^{\omega}\mathbf{J}_s(\omega_m)]\, {}^{\omega}\mathbf{I}_s + {}^{\omega}\mathbf{K}_\tau({}^{\omega}\mathbf{I}_s)\omega_m $$

The structures of matrix $\mathbf{K}_d$ and vector ${}^{\omega}\mathbf{I}_d$ in (23) are:

$$ \mathbf{K}_d = \begin{bmatrix} \left\| \begin{bmatrix} K_{dk} & -K_{ck} \\ K_{ck} & K_{qk} \end{bmatrix} \right\|_{1:2:m_s-2}^{k} & \mathbf{0} \\ \mathbf{0} & K_0 \end{bmatrix}, \qquad {}^{\omega}\mathbf{I}_d = \begin{bmatrix} \left\| \begin{bmatrix} \bar{I}_{dk} \\ \bar{I}_{qk} \end{bmatrix} \right\|_{1:2:m_s-2}^{k} \\ \bar{I}_{m_s} \end{bmatrix}. $$

One can easily proof that the two eigenvalues of the k-th subsystem can be located in $\lambda_{1,2} = -\sigma_c \pm j\omega_c$ using the following parameters:

$$ K_{dk} = \sigma_c\, pL_{dk}, \quad K_{qk} = \sigma_c\, pL_{qk}, \quad K_{ck} = \omega_c\, p\, \sqrt{L_{dk} L_{qk}}. $$

$$\begin{bmatrix} \overset{k}{\left[\begin{matrix} pL_{sd} & 0 \\ 0 & pL_{sq} \end{matrix}\right]}_{1:2:m_s-2} & \mathbf{0} & 0 \\ \mathbf{0} & pL_{s0} & 0 \\ \hline 0 & 0 & J_m \end{bmatrix} \begin{bmatrix} \overset{k}{\left[\begin{matrix} \dot{I}_{dk} \\ \dot{I}_{qk} \end{matrix}\right]}_{1:2:m_s-2} \\ \dot{I}_{m_s} \\ \hline \dot{\omega}_m \end{bmatrix} = - \begin{bmatrix} \overset{k}{\left[\begin{matrix} pR_s & -p^2kq\omega_m L_{sk} \\ p^2kq\omega_m L_{sk} & pR_s \end{matrix}\right]}_{1:2:m_s-2} & \mathbf{0} \\ \mathbf{0} & pR_s \\ \hline -\left[\begin{matrix} K_{dk}(I_{qk}) & K_{qk}(I_{dk}) \end{matrix}\right]_{1:2:m_s-2}^{k} & 0 \end{bmatrix} \begin{bmatrix} \overset{k}{\left[\begin{matrix} K_{dk}(I_{qk}) \\ K_{qk}(I_{dk}) \end{matrix}\right]}_{1:2:m_s-2} \\ 0 \\ \hline b_m \end{bmatrix} \begin{bmatrix} \overset{k}{\left[\begin{matrix} I_{dk} \\ I_{qk} \end{matrix}\right]}_{1:2:m_s-2} \\ I_{m_s} \\ \hline \omega_m \end{bmatrix} + \begin{bmatrix} \overset{k}{\left[\begin{matrix} V_{dk} \\ V_{qk} \end{matrix}\right]}_{1:2:m_s-2} \\ V_{m_s} \\ \hline -\tau_\theta \end{bmatrix} \tag{20}$$

$$\begin{bmatrix} pL_{d1} & 0 & 0 & 0 & 0 & 0 \\ 0 & pL_{q1} & 0 & 0 & 0 & 0 \\ 0 & 0 & pL_{d3} & 0 & 0 & 0 \\ 0 & 0 & 0 & pL_{q3} & 0 & 0 \\ 0 & 0 & 0 & 0 & pL_{s0} & 0 \\ 0 & 0 & 0 & 0 & 0 & J_m \end{bmatrix} \begin{bmatrix} \dot{I}_{d1} \\ \dot{I}_{q1} \\ \dot{I}_{d3} \\ \dot{I}_{q3} \\ \dot{I}_5 \\ \dot{\omega}_m \end{bmatrix} = - \begin{bmatrix} pR_s & -p^2q\omega_m L_{s1} & 0 & 0 & 0 & K_{d1}(I_{q1}) \\ p^2q\omega_m L_{s1} & pR_s & 0 & 0 & 0 & K_{q1}(I_{d1}) \\ 0 & 0 & pR_s & -p^2 3q\omega_m L_{s3} & 0 & K_{d3}(I_{q3}) \\ 0 & 0 & p^2 3q\omega_m L_{s3} & pR_s & 0 & K_{q3}(I_{d3}) \\ 0 & 0 & 0 & 0 & pR_s & 0 \\ -K_{d1}(I_{q1}) & -K_{q1}(I_{d1}) & -K_{d3}(I_{q3}) & -K_{q3}(I_{d3}) & 0 & b_m \end{bmatrix} \begin{bmatrix} I_{d1} \\ I_{q1} \\ I_{d3} \\ I_{q3} \\ I_5 \\ \omega_m \end{bmatrix} + \begin{bmatrix} V_{d1} \\ V_{q1} \\ V_{d3} \\ V_{q3} \\ V_5 \\ -\tau_\theta \end{bmatrix} \tag{21}$$

Fig. 6. Dynamic equations of a MHSM in the transformed frame Σ_ω: equations (20) refer to the generic case m_s and (21) to the case $m_s = 5$.

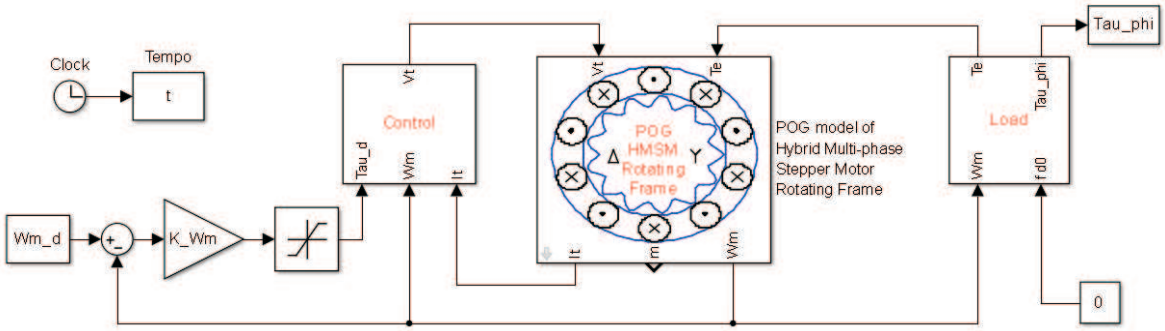

Fig. 7. Simulation of a MHSM: Simulink block scheme.

the desired motor torque τ_{dm} can be expressed as follows:

$$\tau_{dm} = \sum_{k=1:2}^{m_s-2} \alpha_k \tau_{dm}, \qquad \sum_{k=1:2}^{m_s-2} \alpha_k = 1. \tag{24}$$

Coefficients α_k denote the fraction of the desired torque τ_{dm} provided by the k-th subsystem of the motor. The desired currents $\bar{I}_{dk}$ and $\bar{I}_{qk}$ are obtained from the desired torque τ_{dm} using the following relations:

$$\bar{I}_{dk} = \sqrt{\frac{\alpha_k |\tau_{dm}|}{p^2 q\, m_s k |M_{rk}|}}, \qquad \bar{I}_{qk} = \operatorname{sgn}\left(\frac{\tau_{mk}}{M_{rk}}\right) \bar{I}_{dk}. \tag{25}$$

which have been obtained from (22) when $\Phi_k = 0$. These relations are not the optimal ones because they do not take into account the torque generated by the magnet, but are suitable enough for implementing the following simple velocity control law:

$$\tau_{dm} = \text{sat}(\tilde{\tau}_{dm}, \tau_{max}), \qquad \tilde{\tau}_{dm} = K_\omega(\omega_{dm} - \omega_m)$$

where ω_{dm} is the desired motor velocity and $\text{sat}(x, M)$ is the saturation function of variable x within the range $[-M, M]$. The time behaviors of angular velocity ω_m and motor torque τ_m obtained in simulation are shown in blue in Fig. 9: the desired velocity ω_{dm} is reached with a small stead-state error due to the internal friction $b_m\omega_m$ and the external torque τ_e. The time behaviors of the currents I_{d1}, I_{q1}, I_{d3}, I_{d3} and I_5

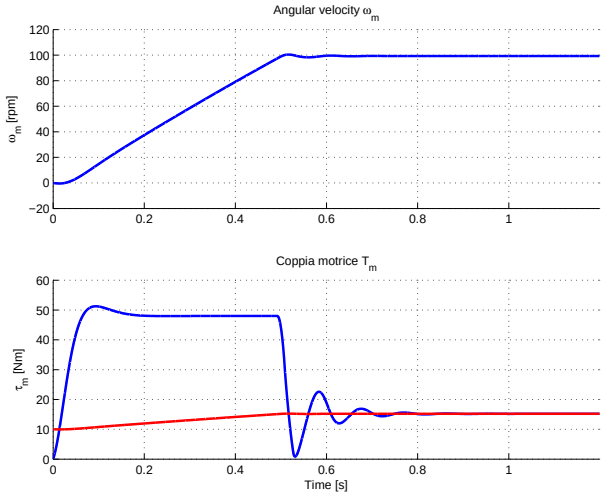

Fig. 9. Angular velocity ω_m and motor torque τ_m.

in the rotating frame Σ_ω are shown in Fig. 10: in the steady-state condition the currents I_{dk} and I_{qk} are constant and the motor generates two different constant torques in the first and in the third internal subsystem. The line voltages V_1, V_2, $\ldots$, V_5 and the line currents I_1, I_2, $\ldots$, I_5 in the final steady-state condition are shown in Fig. 11: the voltage V_1 and the current I_1 have been drawn using a thick blue line

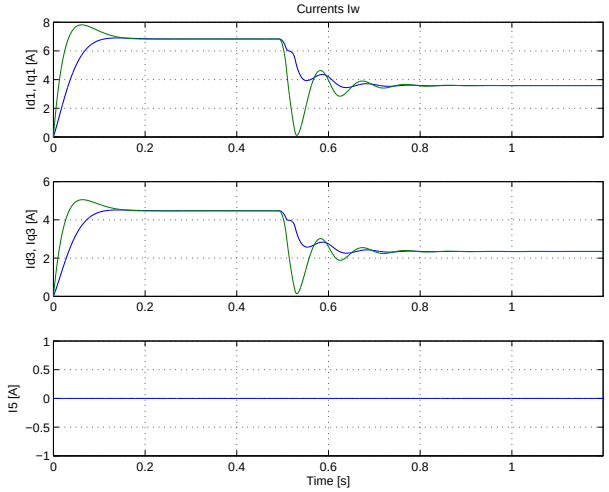

Fig. 10. Currents I_{d1}, I_{q1}, I_{d3}, I_{d3} and I_5 in the rotating frame Σ_ω.

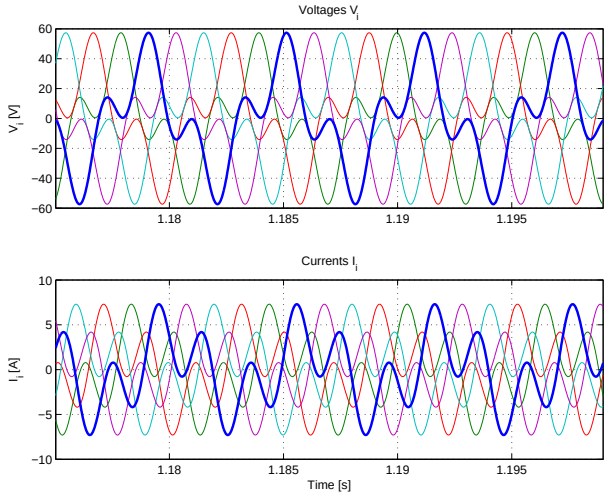

Fig. 11. Line voltages V_1, V_2, ..., V_5 and line currents I_1, I_2, ..., I_5.

to clearly show that these signals are the sum of a first and a third harmonic.

V. Appendix: rotor inductance matrix ${}^t\mathbf{L}_{s\theta}$.

The term $M_{r1}\cos(2q\theta-(q-1)(i+j)\gamma_s)$ in (9) has been obtained referring to the structure $M_{r1}\cos(\alpha\theta-\beta(i+j)\gamma_s)$ and computing the parameters α and β as follows:

1) When $i=j=0$ the term $M_{r1}\cos(\alpha\theta)$ describes the self-inductance coefficient of the first stator phase as a function of electric angle θ. The maximum value of this term is reached when $\theta=\frac{2k\pi}{2q}=\frac{k\pi}{q}$:

$$M_{r1}\cos(\alpha\theta)\Big|_{\theta=\frac{k\pi}{q}}=M_{r1} \quad\rightarrow\quad \alpha\frac{k\pi}{q}=2k\pi \quad\rightarrow\quad \alpha=2q.$$

2) When $i=j$ and $\theta=i\gamma_s-i\gamma_a=i(\gamma_s-\frac{\gamma_s}{q})$ the i-th stator phase self-inductance coefficient $M_{r1}\cos(2q\theta-\beta(i+j)\gamma_s)$ reaches its maximum:

$$M_{r1}\cos(2q\theta-\beta(i+j)\gamma_s)\Big|_{\substack{i=j\\ \theta=i(\gamma_s-\frac{\gamma_s}{q})}}=M_{r1}$$

from which one obtains:

$$2qi(\gamma_s-\frac{\gamma_s}{q})=\beta 2i\gamma_s \quad\rightarrow\quad \beta=q-1.$$

VI. Appendix: flux vector ${}^t\mathbf{\Phi}_c(\theta)$.

The term $\Psi_1\cos(q\theta-h(q-1)\gamma_s)$ in (10) has been obtained referring to the structure $\Psi_1\cos(\alpha\theta-h\beta\gamma_s)$ and computing the parameters α and β as follows:

1) When $h=0$ the term $\Psi_1\cos(\alpha\theta)$ describes the magnetic flux concatenated with first stator phase as a function of the electric angle θ. The maximum value of this term is reached when the electric angle $\theta=\frac{2k\pi}{q}$:

$$\Psi_1\cos(\alpha\theta)\Big|_{\theta=\frac{2k\pi}{q}}=\Psi_1 \quad\rightarrow\quad \alpha\frac{2k\pi}{q}=2k\pi \quad\rightarrow\quad \alpha=q.$$

2) When $\theta=h\gamma_s-h\gamma_a=h(\gamma_s-\frac{\gamma_s}{q})$ the term $\Psi_1\cos(m_r\theta-h\beta\gamma_s)$, which describes the magnetic flux concatenated with the h-th stator phase, reaches its maximum:

$$\Psi_1\cos(q\theta-h\beta\gamma_s)\Big|_{\theta=h\left(\gamma_s-\frac{\gamma_s}{q}\right)}=\Psi_1$$

from which one obtains:

$$qh\left(\gamma_s-\frac{\gamma_s}{q}\right)=h\beta\gamma_s \quad\rightarrow\quad \beta=q-1.$$

References

[1] P.P. Acarnley, Stepping Motors: A guide to Theory and Practice 4th Edition, IEEE, 2002

[2] Oswald, A.; Herzog, H.G., "Investigation of the usability of 2D- and 3D-FEM for a hybrid stepper motor," in Electric Machines and Drives Conference, 2009. IEMDC '09. IEEE International , vol., no., pp.535-542, 3-6 May 2009

[3] Butcher, M.; Masi, A.; Picatoste, R.; Giustiniani, A., "Hybrid Stepper Motor Electrical Model Extensions for Use in Intelligent Drives," in Industrial Electronics, IEEE Transactions on , vol.61, no.2, pp.917-929, Feb. 2014

[4] Bendjedia, M.; Ait-Amirat, Y.; Walther, B.; Berthon, A., "Position Control of a Sensorless Stepper Motor," in Power Electronics, IEEE Transactions on , vol.27, no.2, pp.578-587, Feb. 2012

[5] Hoang Le-Huy; Brunelle, P.; Sybille, G., "Design and implementation of a versatile stepper motor model for simulink's SimPowerSystems," in Industrial Electronics, 2008. ISIE 2008. IEEE International Symposium on , vol., no., pp.437-442, June 30 2008-July 2 2008

[6] R. Zanasi, F. Grossi "Optimal Rotor Flux Shape for Multi-phase Permanent Magnet Synchronous Motors", International Power Electronics and Motion Control Conference, 2008, Poznan, Poland.

[7] R. Zanasi, "The Power-Oriented Graphs Technique: system modeling and basic properties", VPPC 2010, Lille, France, Sept. 2010.

[8] R. Zanasi, F. Grossi, "Differences and common aspects of POG and EMR energy-based graphical techniques", Proc. of IEEE Vehicle Power and Propulsion Conference (VPPC), 2011

[9] M. Fei, R. Zanasi, F. Grossi, "Real and Complex Models of Multi-phase Permanent Magnet Synchronous Motors", IJPEC, International Journal of Power and Energy Conversion, Vol.4, No.2, pp.127 - 151, 2013

[10] M. Fei, R. Zanasi, " Modeling of Multi Open Phase Fault Condition of Multi-phase Permanent Magnet Synchronous Motors", ACEMP 2011 and ELECTROMOTION 2011 - International Aegean Conference on Electric Machines and Power Electronics and Electromotion Joint Conference, Istanbul, Turkey, 08-10 September 2011